A semi-analytic calculation on the atmospheric tau neutrino flux in the GeV to TeV energy range

Fei-Fan Lee and Guey-Lin Lin*

Institute of Physics, National Chiao-Tung University, Hsinchu 300, Taiwan

(Dated: February 2, 2008)

Abstract

We present a semi-analytic calculation on the atmospheric tau neutrino flux in the GeV to TeV energy range. The atmospheric ν_τ flux is calculated for the entire zenith angle range. This flux is contributed by the oscillations of muon neutrinos coming from the two-body π, K decays and the three-body $\mu^\pm$ decays, and the intrinsic tau neutrino flux surviving the oscillations. The uncertainties in our calculations are discussed in detail. The implications of our result are also discussed.

PACS numbers: 95.85.Ry, 14.60.Fg, 14.60.Pq; Keywords: Tau Neutrino, Neutrino Oscillation, Atmospheric Neutrino Flux.

* Contact address: Institute of Physics, National Chiao-Tung University, Hsinchu 300, Taiwan. E-mail: glin@cc.nctu.edu.tw Tel: 886-3-5731984 Fax: 886-3-5720728

I. INTRODUCTION

The flux of atmospheric tau neutrinos in the GeV to TeV energy range comes from both the intrinsic atmospheric ν_τ flux and the flux due to the neutrino flavor oscillation $\nu_\mu \to \nu_\tau$. The importance of understanding such a flux is twofold. First, the detection of atmospheric ν_τ flux is important for confirming the atmospheric $\nu_\mu \to \nu_\tau$ oscillation scenario which is so far established only by the ν_μ disappearance measurement [1]. Second, the atmospheric ν_τ flux is also an important background for the search of astrophysical ν_τ fluxes [2, 3] or exotic ν_τ fluxes such as those arising from dark matter annihilations [4], if an effective tau neutrino astronomy can be developed in the future. The techniques for identifying the tau neutrinos in the GeV to TeV energy range are discussed both in the experiments for atmospheric tau neutrinos [5] and in the accelerator-based neutrino experiments [6, 7]. Due to growing attentions on the direct ν_τ detections, it is important to investigate closely the flux of atmospheric tau neutrinos in such an energy range.

The calculation of atmospheric ν_μ and ν_e fluxes has reached to a rather advanced stage [8]. The upward atmospheric ν_τ flux can be calculated easily from the above ν_μ flux by multiplying the $\nu_\mu \to \nu_\tau$ oscillation probability arising from neutrino propagation inside the Earth. In such a case, the $\nu_\mu \to \nu_\tau$ oscillations in the atmosphere is generally negligible. However, the atmospheric neutrino coming with a zenith angle ξ less than 90° directly arrives at the detector. Hence oscillations of these neutrinos in the atmosphere are precisely the problems one has to deal with. In this regard, an estimation of the atmospheric ν_τ flux is given in Ref. [2] for the two-flavor neutrino oscillation framework [9]. A detailed calculation of this flux in the same neutrino oscillation framework is given in [10] for zenith angles $0 \leq \xi \leq 60^\circ$, where the Earth curvature can be neglected in the calculation. The extension of such a calculation to large zenith angles is important. First of all, the path-length for the neutrino propagation in the atmosphere increases drastically from $\xi = 60^\circ$ to $\xi = 90^\circ$. As a result, the atmospheric ν_τ flux also increases drastically in this zenith angle range by the enhanced $\nu_\mu \to \nu_\tau$ oscillation probabilities. Secondly, the calculation of upward atmospheric ν_τ flux is also important since most of the neutrino telescopes aim at detecting upward neutrino fluxes. In this paper, we shall extend the calculation in [10] to the entire zenith angle range.

The calculations of atmospheric ν_τ flux for zenith angles $60^\circ \leq \xi \leq 90^\circ$ and zenith

angles slightly larger than 90° are much more involved as we shall discuss later. Besides extending our previous calculation to the entire zenith angles, we also extend its validity from the energy range $E_\nu \geq 10$ GeV to the energy range $E_\nu \geq 1$ GeV. This improvement is accomplished by including the muon-decay contribution $\mu^+ \to \bar{\nu}_\mu \nu_e e^+$ and $\mu^- \to \nu_\mu \bar{\nu}_e e^-$ to the intrinsic atmospheric ν_μ flux, in additional to those arising from two-body π and K decays. Such a contribution also generates ν_τ flux by $\nu_\mu \to \nu_\tau$ oscillations. This part of ν_τ flux is non-negligible for $E_\nu \leq 10$ GeV. Furthermore, it contributes to the total ν_τ flux in a growing percentage as the zenith angle ξ increases.

The paper is organized as follows. In Sec. II, we introduce the method for calculating the intrinsic muon and tau neutrino fluxes. Particularly we outline the strategy for dealing with atmospheric neutrino flux for $\xi > 60°$. In Sec. III, we present the atmospheric tau neutrino flux taking into account the neutrino flavor oscillations. We discuss implications of our results in Sec. IV.

II. THE INTRINSIC ATMOSPHERIC NEUTRINO FLUXES

A. Intrinsic atmospheric muon neutrino flux

We follow the approach in [11] for computing the flux of intrinsic atmospheric muon neutrinos which could oscillate into tau neutrinos. This approach computes the flux of muon neutrinos coming from pion and kaon decays. The method for computing muon neutrinos arising from muon decays will be discussed later. The ν_μ flux arising from π decays reads:

$$\begin{aligned}\frac{\mathrm{d}^2 N^\pi_{\nu_\mu}(E,\xi,X)}{\mathrm{d}E\mathrm{d}X} &= \int_E^\infty \mathrm{d}E_N \int_E^{E_N} \mathrm{d}E_\pi \frac{\Theta(E_\pi - \frac{E}{1-r_\pi})}{d_\pi E_\pi (1-r_\pi)} \int_0^X \frac{\mathrm{d}X'}{\lambda_N} P_\pi(E_\pi, X, X') \\ &\quad \times \frac{1}{E_\pi} F_{N\pi}(E_\pi, E_N) \times \exp\left(-\frac{X'}{\Lambda_N}\right) \phi_N(E_N), \end{aligned} \tag{1}$$

where E is the neutrino energy, ξ is the zenith angle in the direction of incident cosmic-ray nucleons, $r_\pi = m_\mu^2/m_\pi^2$, d_π is the pion decay length in units of g/cm^2, λ_N is the nucleon interaction length while Λ_N is the corresponding nucleon attenuation length, and $\phi_N(E_N)$ is the primary cosmic-ray spectrum. For the simplicity in discussions, we only consider the proton component of ϕ_N, which is given by [8]

$$\phi_p(E_p) = 1.49 \cdot \left(E_p + 2.15 \cdot \exp(-0.21\sqrt{E_p})\right)^{-2.74}, \tag{2}$$

in units of $\mathrm{cm}^{-2}\mathrm{s}^{-1}\mathrm{sr}^{-1}\mathrm{GeV}^{-1}$. Since our concerned energy range for the primary cosmic ray flux is between 10^1 GeV and 10^5 GeV per nucleon (corresponding to roughly a neutrino energy range between 10^0 GeV and 10^4 GeV), the contribution by the heavier nuclei on the neutrino flux is between 25% and 40% according to Fig. 7 of Ref. [8]. Hence one expects the eventual atmospheric ν_τ flux is underestimated by 25% to 40% by considering only the proton component of the primary cosmic ray flux. The function $P_\pi(E_\pi, X, X')$ is the probability that a charged pion produced at the slant depth X' ($\mathrm{g/cm}^2$) survives to the depth X ($> X'$), $F_{N\pi}(E_\pi, E_N)$ is the normalized inclusive cross section for $N + \mathrm{air} \to \pi^\pm + Y$ given by [11]:

$$F_{N\pi}(E_\pi, E_N) \equiv \frac{E_\pi}{\sigma_N}\frac{\mathrm{d}\sigma(E_\pi, E_N)}{\mathrm{d}E_\pi} = c_+(1-x)^{p_+} + c_-(1-x)^{p_-}, \tag{3}$$

where $x = E_\pi/E_N$, $c_+ = 0.92$, $c_- = 0.81$, $p_+ = 4.1$, and $p_- = 4.8$. We remark that $c_+(1-x)^{p_+}$ corresponds to the π^+ production while $c_-(1-x)^{p_-}$ corresponds to the π^- production. The kaon contribution to the atmospheric ν_μ flux has the same form as Eq. (1) with an inclusion of the branching ratio $B(K \to \mu\nu) = 0.635$ and appropriate replacements in kinematic factors and the normalized inclusive cross section. In particular, $F_{NK}(E_K, E_N)$ can be parameterized as Eq. (3) with $c_+ = 0.037$, $c_- = 0.045$, $p_+ = 0.87$, and $p_- = 3.5$. Finally the nucleon interaction length, λ_N, and the nucleon attenuation length, Λ_N, are both model dependent. A simplified approach based upon the Feynman scaling render both λ_N and Λ_N energy independent and $Z_{pp} \equiv 1 - \lambda_p/\Lambda_p = 0.263$ [12, 13], whereas a PYTHIA [14] calculation give rise to an energy dependent Z_{pp} [15]. Both results on Z_{pp} are compared in Fig. 1 where we have extrapolated the energy dependent $Z_{pp}(E)$ in Ref. [15] down to $E = 1$ GeV. The above two approaches for calculating the hadronic Z moments also give rise to different results for $Z_{\pi\pi}$, Z_{KK}, $Z_{N\pi}$ and Z_{NK}, where the last two Z-moments are related to the productions of pions and kaons by the nucleon-air collisions. In this paper, we shall only study the Z_{pp} dependence of the atmospheric ν_μ flux (and consequently the atmospheric ν_τ flux) since the dependencies of this flux on $Z_{N\pi}$ and Z_{NK} have been studied in [16]. Furthermore, compared to the Z_{pp} case, the values of $Z_{\pi\pi}$ and Z_{KK} obtained by the Feynman scaling do not differ significantly from those obtained by the PYTHIA calculations, as seen from [15].

To proceed for calculating $\mathrm{d}^2N^\pi_{\nu_\mu}(E, \xi, X)/\mathrm{d}E\mathrm{d}X$, we note that $P_\pi(E_\pi, X, X')$ is given by

[13]

$$P_\pi(E_\pi, X, X') = \exp\left(-\frac{X - X'}{\Lambda_\pi}\right) \cdot \exp\left(-\frac{m_\pi c}{\tau_\pi}\int_{X'}^{X}\frac{\mathrm{d}T}{\rho(T)}\right), \tag{4}$$

where $\Lambda_\pi = 160$ g/cm^2 is the pion attenuation constant, τ_π is the pion lifetime at its rest frame, while $\rho(T)$ is the atmosphere mass density at the slant depth T. For $\xi \leq 60^\circ$, the curvature of the Earth can be neglected so that $\rho(T) = T\cos\xi/h_0$ with $h_0 = 6.4$ km the scale height for an exponential atmosphere. In this approximation, the above survival probability can be written as [11]

$$P_\pi(E_\pi, X, X') = \exp\left(-\frac{X - X'}{\Lambda_\pi}\right) \cdot \left(\frac{X'}{X}\right)^{\epsilon_\pi/E_\pi\cos\xi}, \tag{5}$$

where $\epsilon_\pi = m_\pi c^2 h_0/c\tau_\pi$ is the pion decay constant. Depending on the zenith angle, we apply either Eq. (4) or Eq. (5) to perform the calculations. The kaon survival probability $P_K(E_K, X, X')$ has the same form as $P_\pi(E_\pi, X, X')$ except replacing Λ_π with Λ_K and ϵ_π with ϵ_K. The two-body decay contribution to the atmospheric ν_μ flux is given by the sum of $\mathrm{d}^2N^\pi_{\nu_\mu}(E,\xi,X)/\mathrm{d}E\mathrm{d}X$ and $\mathrm{d}^2N^K_{\nu_\mu}(E,\xi,X)/\mathrm{d}E\mathrm{d}X$.

We recall that Eq. (1) and its corresponding form in the kaon decay case only calculate the flux of muon neutrinos arising from two-body pion and kaon decays. To calculate the contribution from three-body muon decays, it is useful to first obtain the muon flux [11]:

$$\begin{aligned}\frac{\mathrm{d}N^\pi_\mu(E,\xi,X)}{\mathrm{d}E} &= \int_{E'}^{\infty}\mathrm{d}E_N\int_{E'}^{E_N}\mathrm{d}E_\pi\int_0^X \mathrm{d}X'' P_\mu(E, X, X'') \\ &\times \frac{\Theta(E_\pi - E')\Theta(\frac{E'}{r_\pi} - E_\pi)}{d_\pi E_\pi(1 - r_\pi)} \times \int_0^{X''}\frac{\mathrm{d}X'}{\lambda_N}P_\pi(E_\pi, X'', X') \\ &\times \frac{1}{E_\pi}F_{N\pi}(E_\pi, E_N) \times \exp\left(-\frac{X'}{\Lambda_N}\right)\phi_N(E_N),\end{aligned} \tag{6}$$

where E' and E are muon energies at slant depths X'' and X respectively, while $P_\mu(E, X, X'')$ is the muon survival probability given by [13]

$$P_\mu(E, X, X'') = \exp\left[-\frac{m_\mu c}{\tau_\mu}\int_{X''}^{X}\mathrm{d}T\frac{1}{E(T - X'', E')\rho(T)}\right], \tag{7}$$

where τ_μ is the muon lifetime at its rest frame and $E(T - X'', E')$ is the muon energy at the slant depth T with E' the muon energy at its production point X''. For the zenith angle $\xi \leq 60^\circ$, the above survival probability can be written as [11]

$$P_\mu(E, X, X'') = \left(\frac{X''}{X}\frac{E}{E + \alpha(X - X'')}\right)^{\epsilon_\mu/(E\cos\xi + \alpha X\cos\xi)}, \tag{8}$$

with $\epsilon_\mu = m_\mu c^2 h_0/c\tau_\mu$ the muon decay constant and $\alpha \approx 2$ MeV/g/cm^2 characterizing the muon ionization loss in the medium [17]. Since the muons are polarized, it is convenient to keep track of the right-handed and left-handed muon fluxes separately. The probability for a produced μ^- to be right-handed or left-handed is determined by the muon polarization [18, 19]:

$$P_\mu(x) = \frac{1+r_\pi}{1-r_\pi} - \frac{2r_\pi}{(1-r_\pi)x}, \tag{9}$$

with $x = E_\mu/E_\pi$ and $r_\pi = m_\mu^2/m_\pi^2$. Hence $P_{R,L}(x) = \frac{1}{2}\left(1 \pm P_\mu(x)\right)$ are the probabilities for the produced muon to be right-handed or left-handed respectively. The polarization for μ^+ has an opposite sign to that of μ^-. The probabilities $P_{R,L}(x)$ should be inserted into Eq. (6) for obtaining four different components of the muon flux: $\mathrm{d}N^\pi_{\mu^+_R}/\mathrm{d}E$, $\mathrm{d}N^\pi_{\mu^-_R}/\mathrm{d}E$, $\mathrm{d}N^\pi_{\mu^+_L}/\mathrm{d}E$, and $\mathrm{d}N^\pi_{\mu^-_L}/\mathrm{d}E$. There are additional four components of the muon flux arising from the kaon decays. The calculation of these components proceeds in the same way as the pion decay case. The ν_μ flux resulting from the muon flux is then given by [13]

$$\frac{\mathrm{d}^2 N^{\mu^\pm}_{\nu_\mu}(E,\xi,X)}{\mathrm{d}E\mathrm{d}X} = \sum_{s=L,R}\int_E^\infty \mathrm{d}E_\mu \frac{F_{\mu^\pm_s\to\nu_\mu}(E/E_\mu)}{d_\mu(E_\mu,X)E_\mu}\cdot\frac{\mathrm{d}N_{\mu^\pm_s}(E_\mu,\xi,X)}{\mathrm{d}E_\mu}, \tag{10}$$

where $d_\mu(E_\mu,X)$ is the muon decay length in units of g/cm^2 at the slant depth X and $F_{\mu^\pm_s\to\nu_\mu}(E/E_\mu)$ is the decay distribution of $\mu^\pm_s \to \nu_\mu$. Precisely, in the ultra-relativistic limit, one has [13]

$$F_{\mu^-\to\nu_\mu}(y) = g_0(y) + P_\mu g_1(y), \tag{11}$$

with $g_0(y) = 5/3 - 3y^2 + 4y^3/3$, $g_1(y) = 1/3 - 3y^2 + 8y^3/3$. We do not include the charm-hadron decay contribution to the muon neutrino flux. It is shown in Ref. [10] that charm-hadron decays contribute less than 5% to the overall muon neutrino flux for $E_\nu < 10^5$ GeV.

B. Intrinsic atmospheric tau neutrino flux

To completely determine the atmospheric tau neutrino flux, we also need to calculate its intrinsic component. Since the flux of intrinsic atmospheric ν_τ arises from D_s decays, one

calculates this flux by solving the following cascade equations [12]:

$$\begin{aligned}
\frac{\mathrm{d}\phi_p(E,X)}{\mathrm{d}X} &= -\frac{\phi_p}{\lambda_p} + Z_{pp}\frac{\phi_p}{\lambda_p} \\
\frac{\mathrm{d}\phi_{D_s}(E,X)}{\mathrm{d}X} &= -\frac{\phi_{D_s}}{\lambda_{D_s}} - \frac{\phi_{D_s}}{d_{D_s}} + Z_{pD_s}\frac{\phi_p}{\lambda_p} + Z_{D_sD_s}\frac{\phi_{D_s}}{\lambda_{D_s}} \\
\frac{\mathrm{d}\phi_{\nu_\tau}(E,X)}{\mathrm{d}X} &= Z_{D_s\nu_\tau}\frac{\phi_{D_s}}{d_{D_s}},
\end{aligned} \tag{12}$$

where the particle flux $\mathrm{d}\phi_i(E,X)/\mathrm{d}X$ denotes $\mathrm{d}^2N_i(E,X)/\mathrm{d}E\mathrm{d}X$, d_i and λ_i denote particle's decay and interaction length in g/cm^2 respectively, and the Z moments Z_{ij} are defined by

$$Z_{ij}(E_j) \equiv \int_{E_j}^{\infty} \mathrm{d}E_i \frac{\phi_i(E_i)}{\phi_i(E_j)} \frac{\lambda_i(E_j)}{\lambda_i(E_i)} \frac{\mathrm{d}n_{iA\to jY}(E_i,E_j)}{\mathrm{d}E_j}, \tag{13}$$

with $\mathrm{d}n_{iA\to jY}(E_i,E_j) \equiv \mathrm{d}\sigma_{iA\to jY}(E_i,E_j)/\sigma_{iA}(E_i)$. In the decay process, the scattering length λ_i is replaced by the decay length d_i while $\mathrm{d}n_{iA\to jY}(E_i,E_j)/\mathrm{d}E_j$ is replaced by the decay distribution $F_{i\to j}(E_j/E_i)$. In our concerned energy range, the chain of equations in (12) can be easily solved by simplifying the second equation, namely by neglecting terms ϕ_{D_s}/λ_{D_s} and $Z_{D_sD_s}\phi_{D_s}/\lambda_{D_s}$. One obtains

$$\frac{\mathrm{d}^2N_{\nu_\tau}(E,X)}{\mathrm{d}E\mathrm{d}X} = \frac{Z_{pD_s}(E)Z_{D_s\nu_\tau}(E)}{1-Z_{pp}(E)} \cdot \frac{\exp(-X/\Lambda_p)\phi_p(E)}{\Lambda_p}. \tag{14}$$

We use two different values for $Z_{pp} \equiv 1-\lambda_p/\Lambda_p$ as shown in Fig. 1. To determine Z_{pD_s}, it is necessary to calculate $\mathrm{d}\sigma_{pA\to D_sY}(E_p,E_{D_s})/\mathrm{d}E_{D_s}$. Since D_s meson is heavy enough, the above differential cross section is calculable using perturbative QCD [20]. In this work, the next-to-leading order (NLO) perturbative QCD [21, 22] with CTEQ6 parton distribution functions [23] are employed to calculate the differential cross section of $pA \to c\bar{c}$. To obtain $\mathrm{d}\sigma_{pA\to D_sY}(E_p,E_{D_s})/\mathrm{d}E_{D_s}$, we multiply the charm quark differential cross section by the probability factor 13% to account for the fragmentation process $c \to D_s$ [20]. In Fig. 2, we compare our Z_{pD_s} to a previous result obtained by the CTEQ3 parton distribution functions [24]. In the latter work, the NLO pertubative QCD effects are taken into account by the K factor defined by

$$K(E,x_E) = \frac{\mathrm{d}\sigma^{\mathrm{NLO}}(E,x_E)/\mathrm{d}x_E}{\mathrm{d}\sigma^{\mathrm{LO}}(E,x_E)/\mathrm{d}x_E}, \tag{15}$$

where $\mathrm{d}\sigma^{\mathrm{LO}}(E,x_E)/\mathrm{d}x_E$ and $\mathrm{d}\sigma^{\mathrm{NLO}}(E,x_E)/\mathrm{d}x_E$ are leading order and next-to-leading order differential cross sections for $pA \to c\bar{c}$ respectively, with $x_E = E_c/E_p$. For QCD renormalization scale $\mu = m_c$ and the factorization scale $M = 2m_c$, the K factor is fitted to be

[24]

$$K(E, x_E) = 1.36 + 0.42 \ln\left(\ln(E/\mathrm{GeV})\right) + \left(3.40 + 18.7(E/\mathrm{GeV})^{-0.43} - 0.079 \ln(E/\mathrm{GeV})\right) x_E^{1.5}. \quad (16)$$

We apply this K factor to our calculation with CTEQ6 parton distribution functions. Comparing this result with that obtained by applying CTEQ3 parton distribution functions, one acquires an idea on the uncertainty of perturbative QCD approach to the charm hadron production cross section. It is seen from Fig. 2 that both Z moments agree well for energies below TeV. For $E = 10$ TeV, they differ by about 30%.

Besides perturbative QCD approach, there are non-perturbative approach for computing the charm hadron production cross section. In fact, such non-perturbative approaches [25, 26] are motivated to accommodate accelerator data on strange particle productions, which are underestimated by the perturbative QCD approach. It is desirable to apply these approaches to charm hadron productions. The quark-gluon-string-model (QGSM) [25] is a non-perturbative approach based upon the string fragmentation, where the model parameters are tuned to the production cross section of strange particles. The recombination-quark-parton-model (RQPM) [26] is also a phenomenological approach which takes into account the contribution of the intrinsic charm in the nucleon to the charm hadron production cross section. Detailed comparisons of these two models with perturbative QCD approach on the charm hadron productions are given in [27]. It is shown that perturbative QCD approach gives the smallest charm production Z moments. It is clear that the model dependencies on the charm hadron productions affect both the prompt atmospheric muon neutrino flux and the intrinsic atmospheric tau neutrino flux. A detailed study on the model dependencies of the intrinsic atmospheric tau neutrino flux is given in [28]. We shall further discuss these model dependencies after commenting on the Z moment $Z_{D_s\nu_\tau}$.

We note that $Z_{D_s\nu_\tau}$ is related to the energy distributions of the D_s decays into tau neutrinos. One arises from the decay $D_s \to \nu_\tau\tau$, and the other follows from the subsequent tau-lepton decay, $\tau \to \nu_\tau + X$. The latter contribution is calculated using the decay distributions of the decay modes $\tau \to \nu_\tau\rho$, $\tau \to \nu_\tau\pi$, $\tau \to \nu_\tau a_1$ [20, 29], and $\tau \to \nu_\tau l\nu_l$ [12, 13].

The uncertainty of intrinsic atmospheric ν_τ flux due to different approaches for Z_{pp} is negligible. The main uncertainty of this flux is due to the model dependence of the Z-moment Z_{pD_s}. Within the perturbative QCD approach, the dependence of this flux on the parton

distribution functions is shown in Fig. 3. It is easily seen that the intrinsic atmospheric ν_τ flux is not sensitive to parton distribution functions for $E < 10^3$ GeV. However, at $E = 10^4$ GeV, both fluxes differ by almost 50%. Incorporating the non-perturbative approaches for charm hadron productions [25, 26], the uncertainties of intrinsic atmospheric ν_τ flux is depicted in Fig. 4. It is seen that the minimal ν_τ flux in Ref. [28] is consistent with our ν_τ flux calculated by perturbative QCD with CTEQ6 parton distribution functions. On the other hand, the maximal flux shown in Fig. 4 is almost one order of magnitude larger than the minimal one. This maximal flux is given by the RQPM model below 300 GeV while it is given by the QGSM model beyond this energy [30]. We remark that the original minimal and maximal ν_τ fluxes in Ref. [28] correspond to different sets of primary cosmic ray flux, which is considered as one of the uncertainties for the ν_τ flux. However, we have re-scaled these fluxes to a common cosmic ray flux, Eq. (2), used in this paper. We also note that the uncertainty of intrinsic atmospheric ν_τ flux provided by Ref. [28] starts at $E = 100$ GeV, while our calculation of this flux starts at $E = 10$ GeV.

It is interesting to see how much the uncertainty of the intrinsic ν_τ flux could affect the determination of the ν_τ flux taking into account the oscillation effect. In the next section, we shall study this issue with respect to the upward atmospheric ν_τ flux where the oscillation effect is the largest.

III. THE ATMOSPHERIC TAU NEUTRINO FLUX WITH OSCILLATIONS

A. The Downward and Horizontal Atmospheric Tau Neutrino Fluxes

The atmospheric tau neutrino flux can be calculated using

$$\frac{\mathrm{d}\bar{N}_{\nu_\tau}(E,\xi)}{\mathrm{d}E} = \int_0^{X_{\max}(\xi)} \mathrm{d}X \left[\frac{\mathrm{d}^2 N_{\nu_\mu}(E,\xi,X)}{\mathrm{d}E\mathrm{d}X} \cdot P_{\nu_\mu\to\nu_\tau}\left(E, L(X,\xi)\right) + \frac{\mathrm{d}^2 N_{\nu_\tau}(E,\xi,X)}{\mathrm{d}E\mathrm{d}X} \cdot \left(1 - P_{\nu_\mu\to\nu_\tau}\left(E, L(X,\xi)\right)\right) \right], \tag{17}$$

where $P_{\nu_\mu\to\nu_\tau}\left(E, L(X,\xi)\right) \equiv \sin^2 2\theta_{23} \sin^2(1.27\Delta m^2_{31} L/E)$ is the $\nu_\mu \to \nu_\tau$ oscillation probability, assuming a vanishing θ_{13}. We have used the notation $\mathrm{d}\bar{N}_{\nu_\tau}(E,\xi)/\mathrm{d}E$ to denote the atmospheric ν_τ flux taking into account the oscillation effect. The unit of Δm^2_{31} is eV^2 while L and E are in units of km and GeV respectively. A recent SK analysis of the atmospheric

neutrino data implies [1]

$$\Delta m^2_{31} = (1.9 - 3.0) \cdot 10^{-3}\ \text{eV}^2,\ \ \sin^2 2\theta_{23} > 0.9. \tag{18}$$

This is a 90% C.L. range with the best fit values given by $\Delta m^2_{31} = 2.4 \cdot 10^{-3}$ eV^2 and $\sin^2 2\theta_{23} = 1$ respectively.

1. Meson decay contributions

Using the best fit values of neutrino oscillation parameters, we obtain atmospheric tau neutrino fluxes for $\cos\xi = 0.2,\ 0.4,\ \cdots,\ 1$ as depicted in Fig. 5. This set of result is obtained by using an energy-independent Z moment, $Z_{pp} \equiv 1 - \lambda_p/\Lambda_p = 0.263$ mentioned earlier. For the ν_μ flux on the R.H.S. of Eq. (17), we only include the two-body pion and kaon decay contributions. The muon-decay contribution to this flux will be presented later. The intrinsic ν_τ flux in the same equation is taken to be that calculated by perturbative QCD with CTEQ6 parton distribution functions [23]. It is instructive to separately present the oscillated and intrinsic atmospheric ν_τ fluxes corresponding to the two terms on the R.H.S. of Eq. (17). This is done for $\xi = 0^\circ$ in Fig. 6. We see that the oscillated and intrinsic atmospheric ν_τ fluxes cross at $E \simeq 20$ GeV, indicating that the $\nu_\mu \to \nu_\tau$ oscillation effect becomes important for $E < 20$ GeV for such a zenith angle.

We note that the atmospheric ν_τ flux increases as ξ increases from 0° to 90°. There are two crucial factors dictating the angular dependence of such a flux. First, the atmosphere depth traversed by the cosmic ray particles increases as the zenith angle ξ increases. Second, the atmospheric muon neutrinos are on-average produced more far away from the ground detector for a larger zenith angle, implying a larger $\nu_\mu \to \nu_\tau$ oscillation probability. In fact, the neutrino path-length dependencies on the zenith angle ξ and the neutrino energy E have been studied carefully by the Monte-Carlo simulation [31]. Our semi-analytic approach reproduces these dependencies very well. It is found that, for $E = 10$ GeV and $\cos\xi = 1$ ($\xi = 0^\circ$), the average neutrino path-length from the ν_μ production point to the ground detector is 14 km. The average neutrino path-length increases to 45 km and 650 km for $\xi = 66^\circ$ ($\cos\xi = 0.4$) and $\xi = 90^\circ$ respectively. The huge path-length of horizontal neutrinos makes the ν_τ flux in this direction two orders of magnitude larger than the downward ν_τ flux. It is also interesting to note that the horizontal ν_τ flux for E approaching 1 GeV begins

to show oscillatory behavior. This is because, for $E = 1$ GeV and $\Delta m^2_{31} = 2.4 \cdot 10^{-3}$ eV^2, $L_{\rm osc} \equiv 4E/\Delta m^2_{31} \approx 330$ km which is already shorter than the average neutrino path-length at this zenith angle.

We stress that our calculation procedures for $\cos\xi > 0.5$ and $\cos\xi < 0.5$ are different. In the former case, the curvature of the Earth can be neglected and the pion or kaon survival probability in the atmosphere is approximated by Eq. (5). This is the approach we adopted in Ref. [10]. For $\cos\xi < 0.5$, i.e., $\xi > 60^\circ$, we use Eq. (4) for the meson survival probability. In this case the calculation is much more involved as the meson survival probability in Eq. (4) contains an additional integration. It has been pointed out in Ref. [31] that one may apply Eq. (5) for calculating the path-length distribution of neutrinos for $\xi > 60^\circ$ so long as one replaces $\cos\xi$ by $\cos_{\rm eff}\xi$, where the latter is a fitted function of the former. Precisely speaking, by fitting the analytic calculation based upon Eq. (5) [13] to the Monte-Carlo calculation, the relations between $\cos\xi$ and $\cos_{\rm eff}\xi$ can be found, which are tabulated in [31]. Extrapolating such a relation, we find that $\cos_{\rm eff}\xi = 0.05$ for $\cos\xi = 0$. Using this $\cos_{\rm eff}\xi$ with Eq. (5), we also calculate the atmospheric ν_τ flux. The result is compared with that obtained by the full calculation (applying Eq. (4)) as shown in Fig. 7. Both results agree very well. Such an agreement makes our calculation compelling and also validates the above extrapolation on $\cos_{\rm eff}\xi$.

We have so far computed the atmospheric neutrino flux with an energy independent Z moment, $Z_{pp} \equiv 1 - \lambda_p/\Lambda_p = 0.263$. It is important to check the sensitivity of atmospheric ν_τ flux on the values of Z_{pp}. We recall that different results for Z_{pp} are shown in Fig. 1. At energies between 10^2 GeV and 10^3 GeV, the values of Z_{pp} generated by PYTHIA [14] slightly depend on the energy and roughly twice larger than the value we have so far used for calculations. We check the effect of Z_{pp} by calculating the atmospheric ν_τ flux with the PYTHIA-generated Z_{pp}. The comparison of this result with the earlier one obtained by setting $Z_{pp} = 0.263$ is shown in Fig. 8 for $\xi = 0^\circ$ and Fig. 9 for $\xi = 90^\circ$. For $\xi = 0^\circ$, two set of results do not exhibit noticeable difference until $E \geq 10$ GeV. At $E = 100$ GeV, they differ by 45%. For $\xi = 90^\circ$, two results differ by 46% at $E = 1$ GeV while they differ by 29% at $E = 100$ GeV. Obviously, the behavior of Z_{pp} is one of the major uncertainties for determining the atmospheric ν_τ flux.

2. Muon-Decay contributions

We have stated that the muon-decay contributions to ν_μ is non-negligible for neutrino energies less than 10 GeV. Such ν_μ's can oscillate into ν_τ's during their propagations in the atmosphere. The calculation of such a flux according to Eqs. (6) and (10) is rather involved. However, a simple approximation as presented below gives a rather accurate result for this flux.

The calculation of ν_μ spectrum due to muon decays requires the knowledge of muon polarizations. The muon polarization however depends on the ratio of muon momentum to the momentum of parent pion or kaon as indicated by Eq. (9). It is straightforward to calculate the average muon polarization at any slant depth X provided the energy spectrum of the parent pion or kaon is known at that point. For the downward case ($\xi = 0^\circ$), it is known from the previous section that the muons are most likely produced at around 14 km from the ground detector. At that point, the pion and kaon fluxes can be approximately parameterized as $\phi_\pi(E_\pi) = 10^{-3.15} \cdot E_\pi^{-2.02}$ and $\phi_K(E_K) = 10^{-5.11} \cdot E_K^{-1.74}$ in units of $\mathrm{cm}^{-2}\mathrm{s}^{-1}\mathrm{sr}^{-1}\mathrm{GeV}^{-1}$ for meson energies between 1 and few tens of GeV. We do not distinguish $\pi^-(K^-)$ from $\pi^+(K^+)$ in the above fittings. Although the spectra are charge dependent, the resulting absolute values of μ^+ polarization and μ^- polarization differ by only 10% for E_μ up to few tens of GeV [13]. From Eq. (9), and the above pion and kaon spectra, we obtain $\langle P^\pi_{\mu^-} \rangle = 0.35$, $\langle P^K_{\mu^-} \rangle = 0.95$. Therefore μ^- coming from the π^- decays are 67% right-handed polarized and 33% left-handed polarized. On the other hand, μ^- coming from K^- decays are 98% right-handed polarized and only 2% left-handed polarized. The muons produced by meson decays lose energies before they decay into neutrinos. The decay distribution for $\mu^- \to \nu_\mu$ is given by Eq. (11). The average momentum fraction $\langle y \rangle$ of muon neutrinos are 0.3 and 0.4 from decays of right-handed μ^- and left-handed μ^- respectively. Following a similar procedure, one can determine the polarization and decay distributions of μ^+. Finally, to calculate the spectrum of muon neutrinos arising from muon decays, we use the approximation of replacing $F_{\mu_s^\pm \to \nu_\mu}(E/E_\mu)$ with $\delta(E/E_\mu - \langle y \rangle)$ in Eq. (10).

To check the validity of the above approximation, we compare our result on the fraction of muon decay contribution to the overall ν_μ flux with that given by Ref. [13] for $\cos\xi = 0.4$, i.e., $\xi = 66^\circ$. At this zenith angle, most of the muons are produced roughly 45 km from the detector. The pion and kaon fluxes at this point are fitted to be $\phi_\pi(E_\pi) = 10^{-3.65} \cdot E_\pi^{-1.88}$ and

$\phi_K(E_K) = 10^{-5.57} \cdot E_K^{-1.69}$ in units of $\mathrm{cm}^{-2}\mathrm{s}^{-1}\mathrm{sr}^{-1}\mathrm{GeV}^{-1}$. This gives rise to $\langle P^{\pi}_{\mu^-} \rangle = 0.34$, $\langle P^{K}_{\mu^-} \rangle = 0.94$. Following the procedure in the downward case, we obtain the muon neutrino flux from the muon decays. At $E = 1$ GeV, the fraction of muon-decay contributions to the overall ν_μ flux is 44% while the fraction decreases to 17% at $E = 10$ GeV. In Ref. [13], the corresponding fractions are 47% and 18% respectively. Both set of fractions agree rather well.

Since our approximation works well for calculating the muon-decay contributions to the atmospheric ν_μ flux, we proceed to calculate the resulting atmospheric ν_τ flux with Eq. (17). Specifically we only need to include the first term on the R.H.S. of Eq. (17) because the second term has already been included in the two-body decay contribution. In Fig. 10, those atmospheric ν_τ fluxes resulting from oscillations of ν_μ's generated by both two- and three-body decays (muon decays) are compared with those resulting from the oscillations of ν_μ's generated only by two-body decays. As expected, the three-body decay contribution is non-negligible for $E \leq 10$ GeV. Quantitatively, for $\xi = 0^\circ$ and $E = 1$ GeV, 24% of the total atmospheric ν_τ flux is from the oscillations of ν_μ's originated from the muon decays. At $E = 10$ GeV, only 2.9% of the total atmospheric ν_τ flux comes from the same source. For $\xi = 66^\circ$, the three-body decay contribution gives rise to 36% and 8.9% of the total atmospheric ν_τ flux at $E = 1$ GeV and $E = 10$ GeV respectively. Finally, for $\xi = 90^\circ$, the three-body decay contribution to the total atmospheric ν_τ flux is most significant. It contributes to 53%, 46%, and 39% of the total atmospheric ν_τ flux at $E = 1$ GeV, 10 GeV and 20 GeV respectively. To calculate the three-body decay contribution to ν_μ flux at $\xi = 90^\circ$, we have used Eq. (5) for the meson survival probability with $\cos_{\mathrm{eff}} \xi = 0.05$ and a overall factor $C \approx 1.40$ to fix the normalization of the flux [31].

B. The Upward Atmospheric Tau Neutrino Flux

The upward atmospheric ν_τ fluxes are enhanced compared to those of other directions since the average neutrino path lengths in such case are larger. Therefore the observations of astrophysical tau neutrinos in upward directions are subject to more serious background problems. However, observing the atmospheric tau neutrinos is interesting in its own right. The atmospheric tau neutrino flux for $\cos\xi = -0.2$ is shown in Fig. 11. The effect of $\nu_\mu \to \nu_\tau$ oscillation is evident for below TeV energies. This is seen from the crossing point

of intrinsic and oscillated atmospheric ν_τ fluxes at $E \simeq 700$ GeV. The atmospheric ν_τ flux shows oscillatory behavior for $E \leq 10$ GeV. For $\cos\xi < -0.2$, such an oscillatory behavior is even more significant. In such a case, it is more practical to study the averaged flux. We average the atmospheric ν_τ flux for the zenith angle range $-1 \leq \cos\xi \leq -0.4$, as shown in Fig. 12. Due to uncertainties of the intrinsic atmospheric ν_τ flux as discussed in Ref. [28], the atmospheric ν_τ flux taking into account the oscillation effect also contains uncertainties beginning at a few hundred GeV's. In the same figure, we also plot the corresponding atmospheric ν_μ flux. The ν_μ and ν_τ fluxes are comparable for $E < 40$ GeV. In such a case, the footprint of ν_τ might be identified by studying the energy spectra of shower events induced by neutrino interactions [5]. At $E = 10^4$ GeV, the ν_μ flux is approximately 30 times larger than the maximal ν_τ flux. We note that the maximal and minimal ν_τ fluxes begin to differ at $E = 500$ GeV. At $E = 1$ TeV, the maximal flux is 3 times larger than the minimal one. The ratio of maximal flux to the minimal one increases to 14 at $E = 10$ TeV. We remark that the upward atmospheric ν_τ flux is also calculated in Ref. [5] with $\sin^2 2\theta_{23} = 1$ and $\Delta m^2_{31} = 10^{-2},\ 10^{-2.5},\ 10^{-3}$ eV^2 respectively. Here we have done the calculation with the best fit value of $\sin^2 2\theta_{23}$ and Δm^2_{31} taken from [1]. Furthermore we include the contribution of intrinsic atmospheric ν_τ flux and its associated uncertainties.

IV. DISCUSSION AND CONCLUSION

The understanding of atmospheric ν_τ flux is important for exploring the tau neutrino astronomy [2, 10]. As mentioned earlier, an estimation of the atmospheric ν_τ flux has been given in Ref. [2] while a detailed calculation of this flux for zenith angles $0 \leq \xi \leq 60^\circ$ is given in Ref. [10]. In these works, comparisons of the galactic-plane ν_τ flux with the atmospheric ν_τ flux are also made for illustrating the possibility of the tau neutrino astronomy. Now that we have obtained a complete result of the atmospheric ν_τ flux for the entire zenith angle range, we compare this flux with two astrophysical fluxes: the galactic-plane tau neutrino flux just mentioned and the cosmological ν_τ flux due to neutralino dark matter annihilations [32]. The comparison is depicted in Fig. 13 where the flux of galactic-plane tau neutrinos is taken from the calculation of Ref. [10]. One can see that the galactic-plane ν_τ flux dominates over the downward ($\xi = 0^\circ$) atmospheric ν_τ flux for E greater than a few GeV. Hence, in this direction, it is possible to observe the flux of galactic-plane tau neutrinos in the GeV energy

range. For near horizontal directions, the atmospheric ν_τ flux grows rapidly with zenith angles. Therefore, for $\xi = 90^\circ$, the energy threshold for galactic-plane tau neutrino flux to dominate over its atmospheric counterpart is pushed up to $E \simeq 100$ GeV. We further see that the galactic-plane ν_τ flux does not dominate the upward atmospheric ν_τ background ($-1 \leq \cos\xi \leq -0.4$) until $E = 500$ GeV. However, it is noteworthy that, in the muon neutrino case, galactic-plane neutrino flux is overwhelmed by the atmospheric background until $E_\nu > 10^6$ GeV [33]. Such a difference between ν_μ and ν_τ shows the promise of the tau neutrino astronomy in the GeV energy range as pointed out in [2, 10]. From Fig. 13, it is also clear that the atmospheric ν_τ flux is a non-negligible background to the cosmological tau neutrino flux due to neutralino dark matter annihilations [32]. In fact, two fluxes are comparable in the downward direction while the atmospheric ν_τ flux dominates in horizontal and upward directions.

In summary, we have presented a semi-analytical calculation on the atmospheric ν_τ flux in the GeV to TeV energy range for downward, upward, and horizontal directions. The atmospheric ν_τ flux at $\xi = 90^\circ$ is two orders of magnitude larger than the corresponding flux at $\xi = 0^\circ$ for $1 \leq E/\text{GeV} \leq 10$. On the other hand, the fluxes with zenith angles between 0 and 90 degrees merge for $E \geq 700$ GeV, provided that the intrinsic atmospheric ν_τ flux is calculated with perturbative QCD. Should one adopt a non-perturbative model for the intrinsic ν_τ flux, the resulting ν_τ fluxes on Earth at different zenith angles would merge at an energy lower than 700 GeV. We have observed that the upward atmospheric ν_τ fluxes show oscillatory behaviors. For the averaged flux with $-1 \leq \cos\xi \leq -0.4$, the atmospheric ν_τ flux is found to be comparable to the atmospheric ν_μ flux for $E < 40$ GeV. The comparison of this flux with the horizontal atmospheric ν_τ flux is also interesting. Two fluxes are in fact comparable for $E < 10$ GeV. This shows that the $\nu_\mu \to \nu_\tau$ oscillation is already quite significant in the horizontal direction for such an energy range. Nevertheless, the upward atmospheric ν_τ flux takes over from $E \geq 10$ GeV until $E \simeq 3$ TeV where two fluxes merge again. Concerning the uncertainties in our calculations, we have studied the dependencies of atmospheric ν_τ flux on the Z moment Z_{pp} for representative zenith angles $\xi = 0^\circ$ and $\xi = 90^\circ$. We have also discussed in detail the uncertainty of intrinsic atmospheric ν_τ flux due to different models for charm hadron productions. The consequence of such a uncertainty on the determination of oscillated ν_τ flux is studied as well. Concerning the technique for calculating the atmospheric ν_τ flux from large zenith angles, we have verified the validity

of using $\cos_{\rm eff}\,\xi$ in Eq. (5) to calculate the atmospheric ν_τ flux for $\xi > 60^\circ$. In particular, we have extrapolated the results in Ref. [31] to $\xi = 90^\circ$ and demonstrate that the choice $\cos_{\rm eff}(\xi = 90^\circ) = 0.05$ reproduces well the atmospheric ν_τ flux obtained by a full calculation using Eq. (4).

Acknowledgements

This work is supported by the National Science Council of Taiwan under the grant number NSC 93-2112-M-009-001.

---

[1] For a recent result, see Y. Ashie *et al.* [Super-Kamiokande Collaboration], Phys. Rev. Lett. **93**, 101801 (2004) [arXiv:hep-ex/0404034].

[2] H. Athar, Mod. Phys. Lett. A **19**, 1171 (2004).

[3] H. Athar and C. S. Kim, Phys. Lett. B **598**, 1 (2004) [arXiv:hep-ph/0407182].

[4] For a recent review, see G. Bertone, D. Hooper and J. Silk, Phys. Rept. **405**, 279 (2005) [arXiv:hep-ph/0404175].

[5] T. Stanev, Phys. Rev. Lett. **83**, 5427 (1999) [arXiv:astro-ph/9907018].

[6] A. Zalewska [ICARUS Collaboration], Acta Phys. Polon. B **35**, 1949 (2004).

[7] J. Campagne, Eur. Phys. J. C **33**, S837 (2004).

[8] T. K. Gaisser and M. Honda, Ann. Rev. Nucl. Part. Sci. **52**, 153 (2002) [arXiv:hep-ph/0203272].

[9] For an estimation of the same flux in the three-flavor neutrino oscillation framework, see H. Athar, arXiv:hep-ph/0411303.

[10] H. Athar, F. F. Lee and G. L. Lin, Phys. Rev. D **71**, 103008 (2005) [arXiv:hep-ph/0407183].

[11] T. K. Gaisser, Astropart. Phys. **16**, 285 (2002) [arXiv:astro-ph/0104327].

[12] *Cosmic Rays and Particle Physics*, T. K. Gaisser, Cambridge University Press (1992).

[13] P. Lipari, Astropart. Phys. **1**, 195 (1993).

[14] T. Sjöstrand, Comput. Phys. Commun. **82**, 74 (1994).

[15] M. Thunman, G. Ingelman and P. Gondolo, Astropart. Phys. **5**, 309 (1996) [arXiv:hep-ph/9505417].

[16] V. Agrawal, T. K. Gaisser, P. Lipari and T. Stanev, Phys. Rev. D **53**, 1314 (1996) [arXiv:hep-ph/9509423].

[17] B. Rossi, High Energy Particles (Prentice Hall, Englewood Cliffs, NJ, USA, 1952).

[18] S. M. Barr, T. K. Gaisser, P. Lipari and S. Tilav, Phys. Lett. B **214**, 147 (1988).

[19] G. Barr, T. K. Gaisser and T. Stanev, Phys. Rev. D **39**, 3532 (1989).

[20] L. Pasquali and M. H. Reno, Phys. Rev. D **59**, 093003 (1999) [arXiv:hep-ph/9811268].

[21] P. Nason, S. Dawson and R. K. Ellis, Nucl. Phys. B **327**, 49 (1989) [Erratum-ibid. B **335**, 260 (1990)].

[22] M. L. Mangano, P. Nason and G. Ridolfi, Nucl. Phys. B **373**, 295 (1992).

[23] J. Pumplin, D. R. Stump, J. Huston, H. L. Lai, P. Nadolsky and W. K. Tung, JHEP **0207**, 012 (2002) [arXiv:hep-ph/0201195].

[24] L. Pasquali, M. H. Reno and I. Sarcevic, Phys. Rev. D **59**, 034020 (1999) [arXiv:hep-ph/9806428].

[25] A. B. Kaidalov and O. I. Piskunova, Z. Phys. C **30**, 145 (1986); L. V. Volkova, W. Fulgione, P. Galeotti and O. Saavedra, Nuovo Cim. C **10**, 465 (1987).

[26] E. V. Bugaev, A. Misaki, V. A. Naumov, T. S. Sinegovskaya, S. I. Sinegovsky and N. Takahashi, Phys. Rev. D **58**, 054001 (1998) [arXiv:hep-ph/9803488].

[27] C. G. S. Costa, Astropart. Phys. **16**, 193 (2001) [arXiv:hep-ph/0010306].

[28] C. G. S. Costa, F. Halzen and C. Salles, Phys. Rev. D **66**, 113002 (2002) [arXiv:hep-ph/0104039].

[29] B. A. Li, Phys. Rev. D **52**, 5165 (1995) [arXiv:hep-ph/9504304].

[30] C. G. S. Costa and C. Salles, arXiv:hep-ph/0105271.

[31] T. K. Gaisser and T. Stanev, Phys. Rev. D **57**, 1977 (1998) [arXiv:astro-ph/9708146].

[32] D. Elsaesser and K. Mannheim, Astropart. Phys. **22**, 65 (2004) [arXiv:astro-ph/0405347].

[33] H. Athar, K. Cheung, G. L. Lin and J. J. Tseng, Eur. Phys. J. C **33**, S959 (2004) [arXiv:astro-ph/0311586].

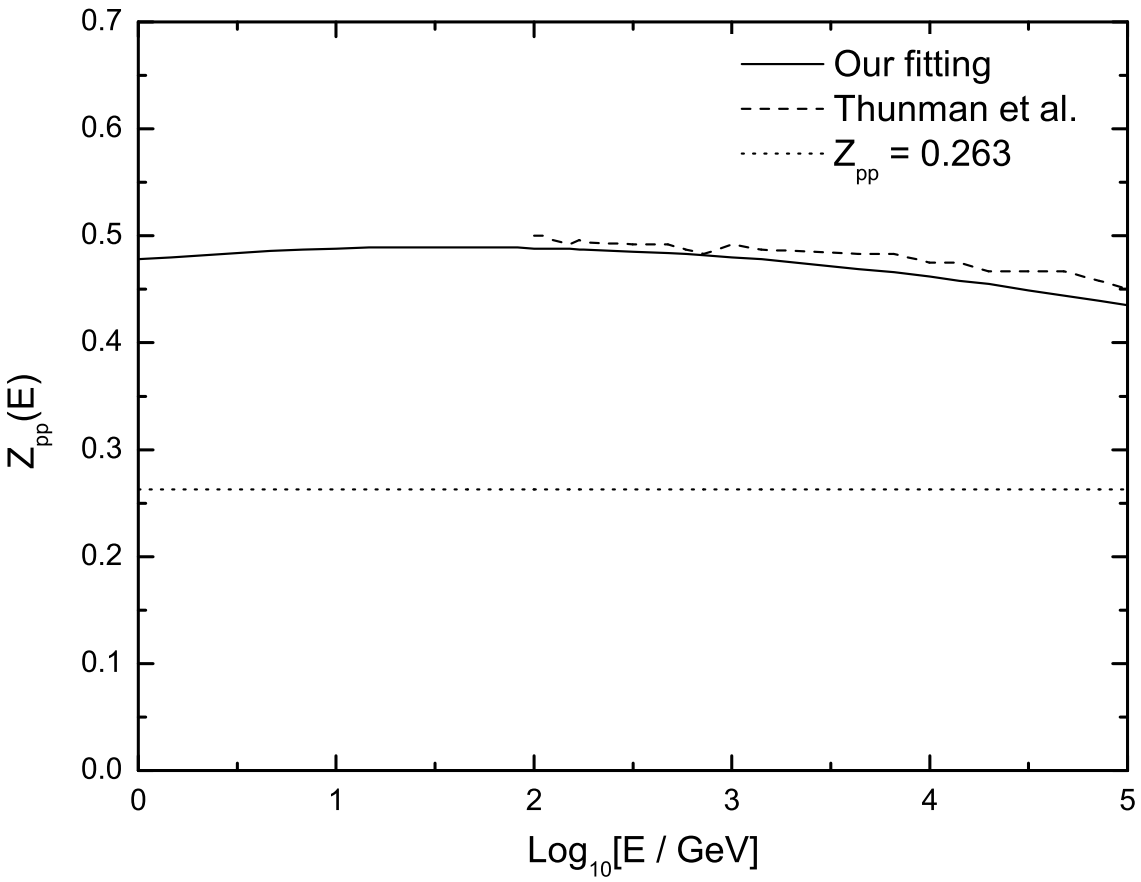

FIG. 1: The comparison of Z_{pp} obtained by assuming the Feynman scaling [12] and that obtained by PYTHIA [15]. Our extrapolation of the latter result is also shown.

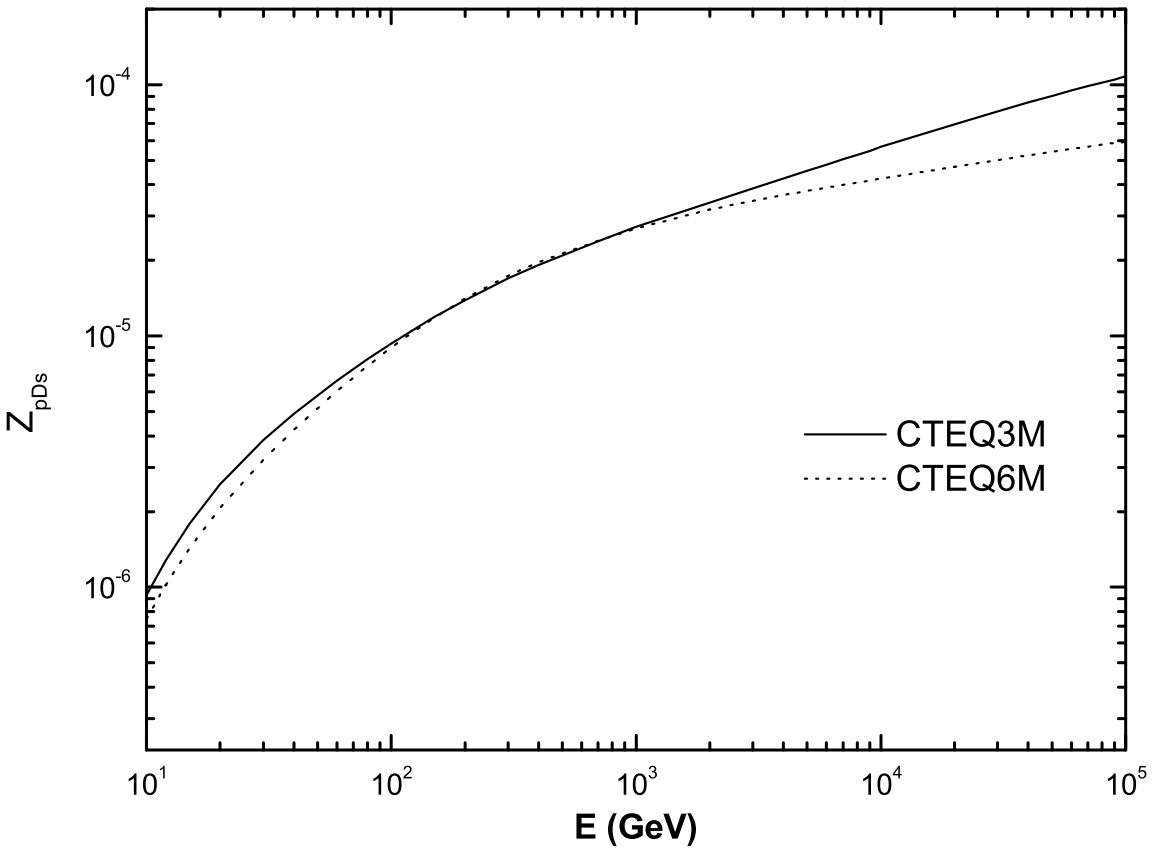

FIG. 2: The Z moment Z_{pD_s} obtained by perturbative QCD with CTEQ3 and CTEQ6 parton distribution functions respectively.

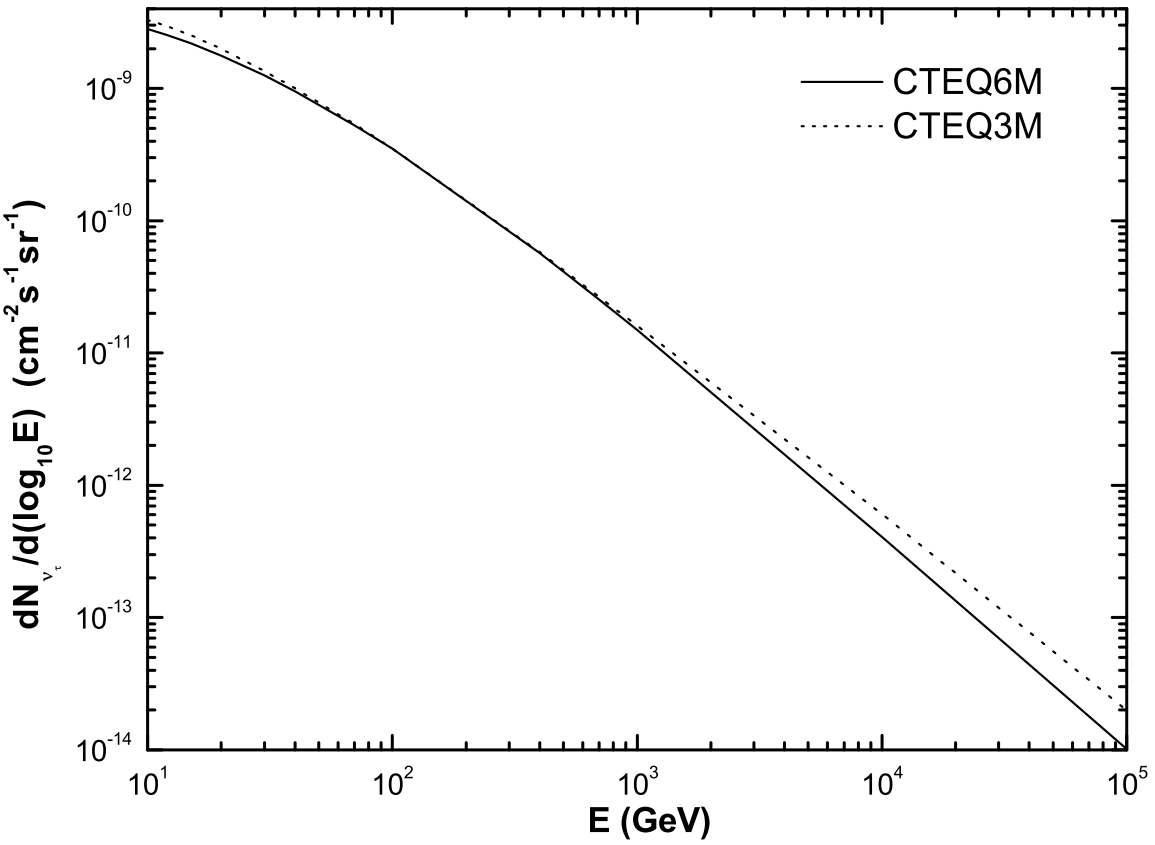

FIG. 3: The comparison of intrinsic atmospheric ν_τ fluxes calculated by perturbative QCD with CTEQ3 and CTEQ6 parton distribution functions respectively.

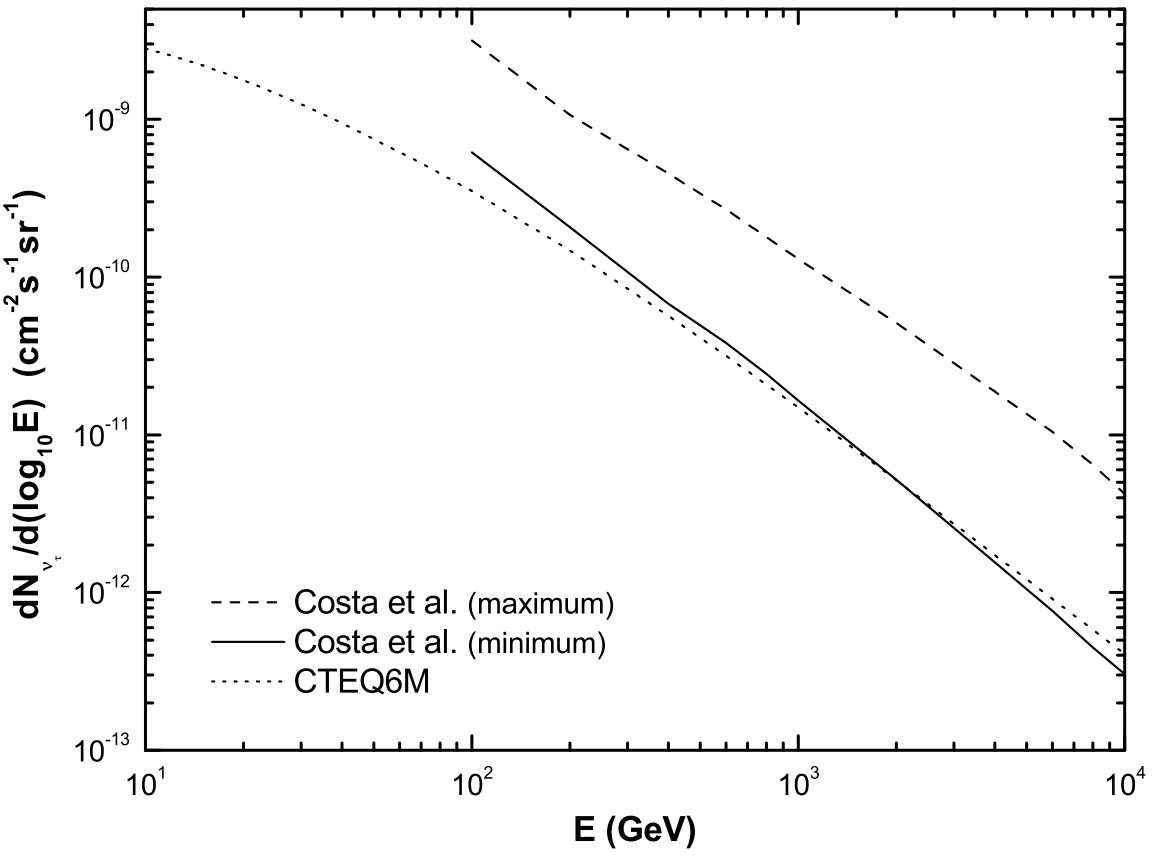

FIG. 4: The model dependencies of intrinsic atmospheric ν_τ flux. The minimal flux from Ref. [28] is given by perturbative QCD. The maximal flux from the same reference is given by RQPM model for $E \leq 300$ GeV, and by QGSM model for $E > 300$ GeV.

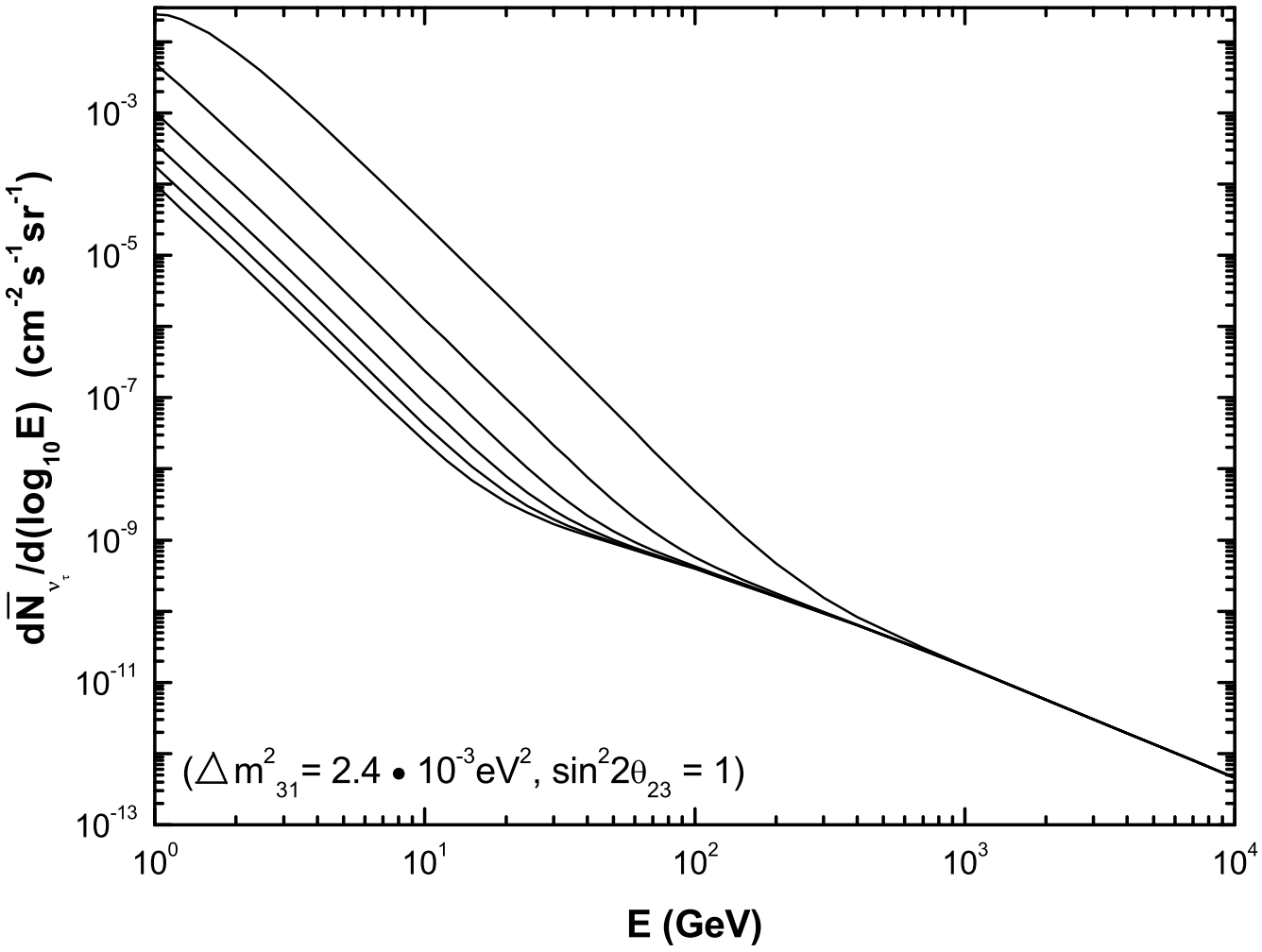

FIG. 5: The atmospheric ν_τ flux for $\cos\xi = 0,\ 0.2,\ 0.4,\ 0.6,\ 0.8$ and 1 (from top to bottom) with $\sin^2 2\theta_{23} = 1$, $\Delta m^2_{31} = 2.4 \cdot 10^{-3}$ eV^2, and $Z_{pp} = 0.263$.

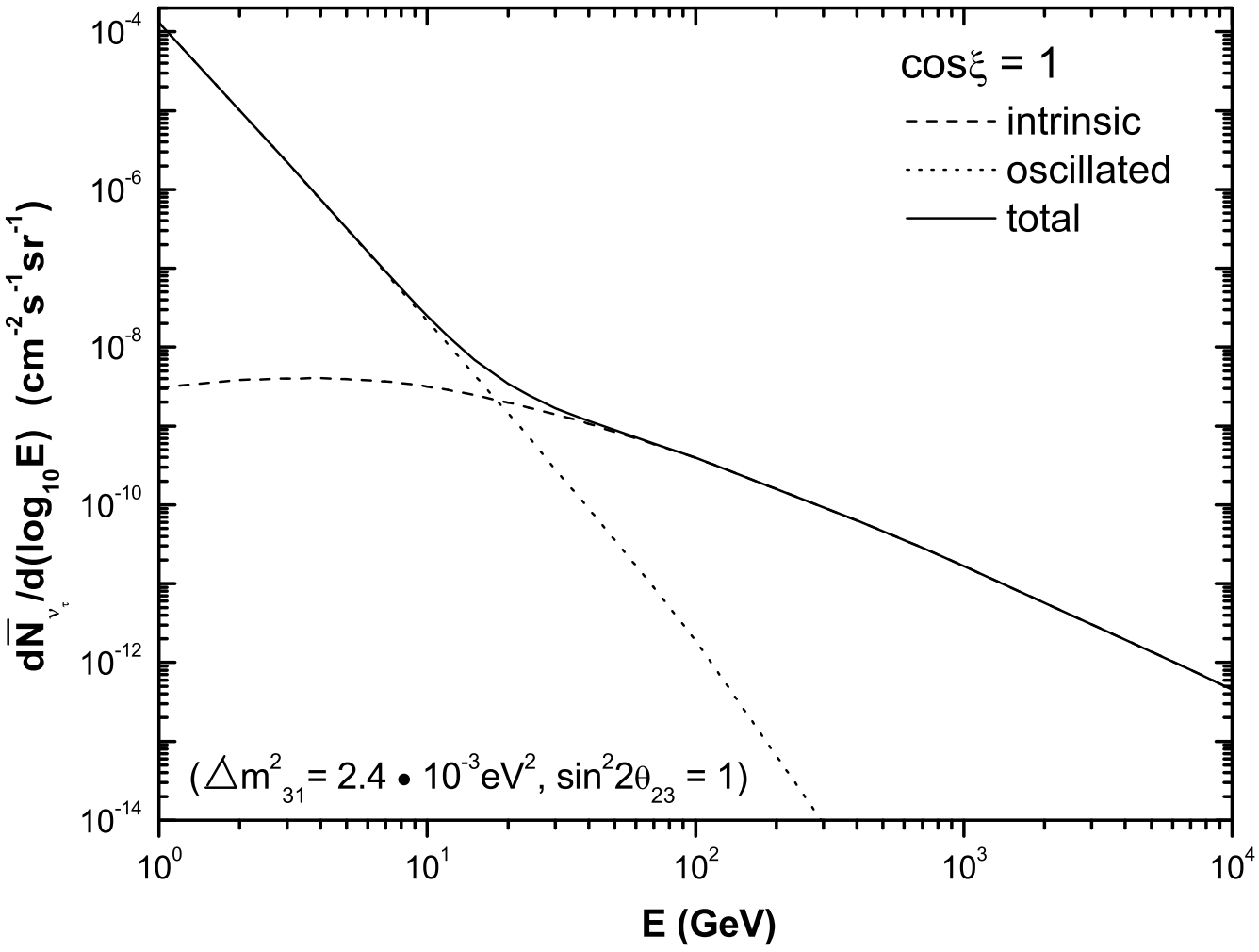

FIG. 6: The downward atmospheric ν_τ flux (solid line) as the sum of its oscillated (dotted line) and intrinsic (dashed line) components.

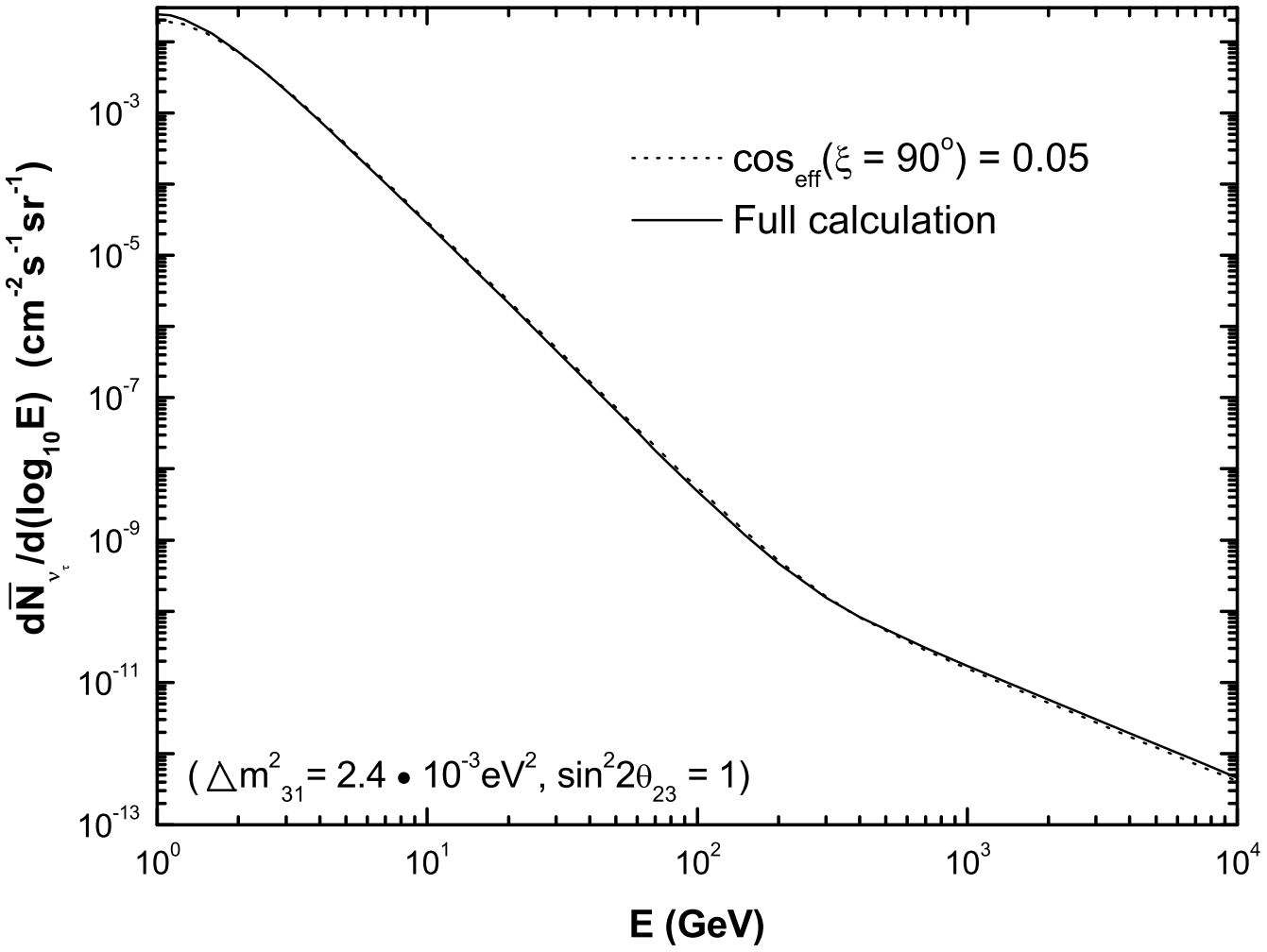

FIG. 7: The comparison of atmospheric ν_τ flux obtained by using $\cos_{\rm eff}\,\xi$ and that obtained by the full calculation for $\xi = 90^\circ$.

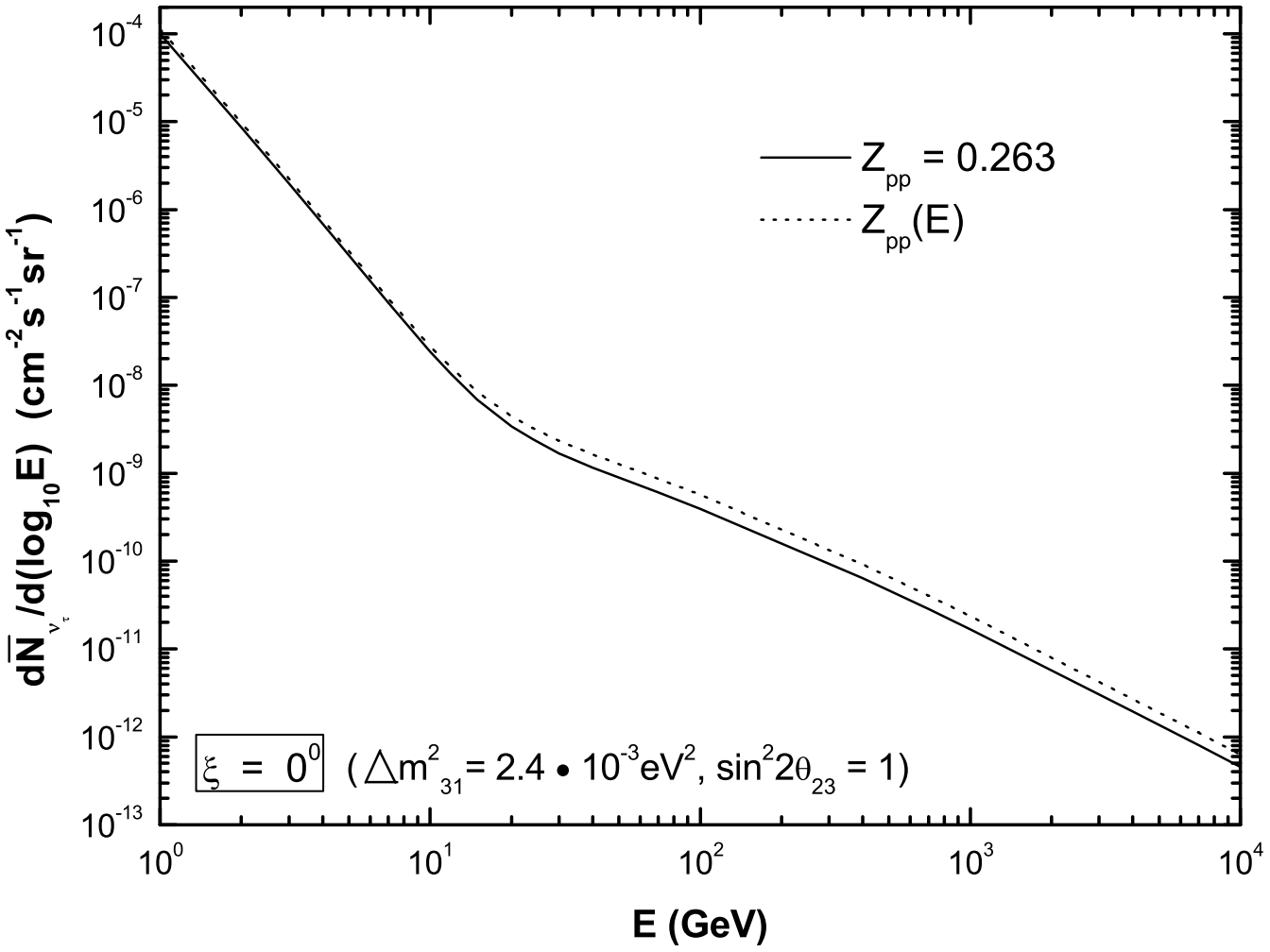

FIG. 8: The comparison of atmospheric ν_τ fluxes calculated from a constant Z_{pp} [12, 13] and an energy-dependent Z_{pp} [15] for $\xi = 0^\circ$.

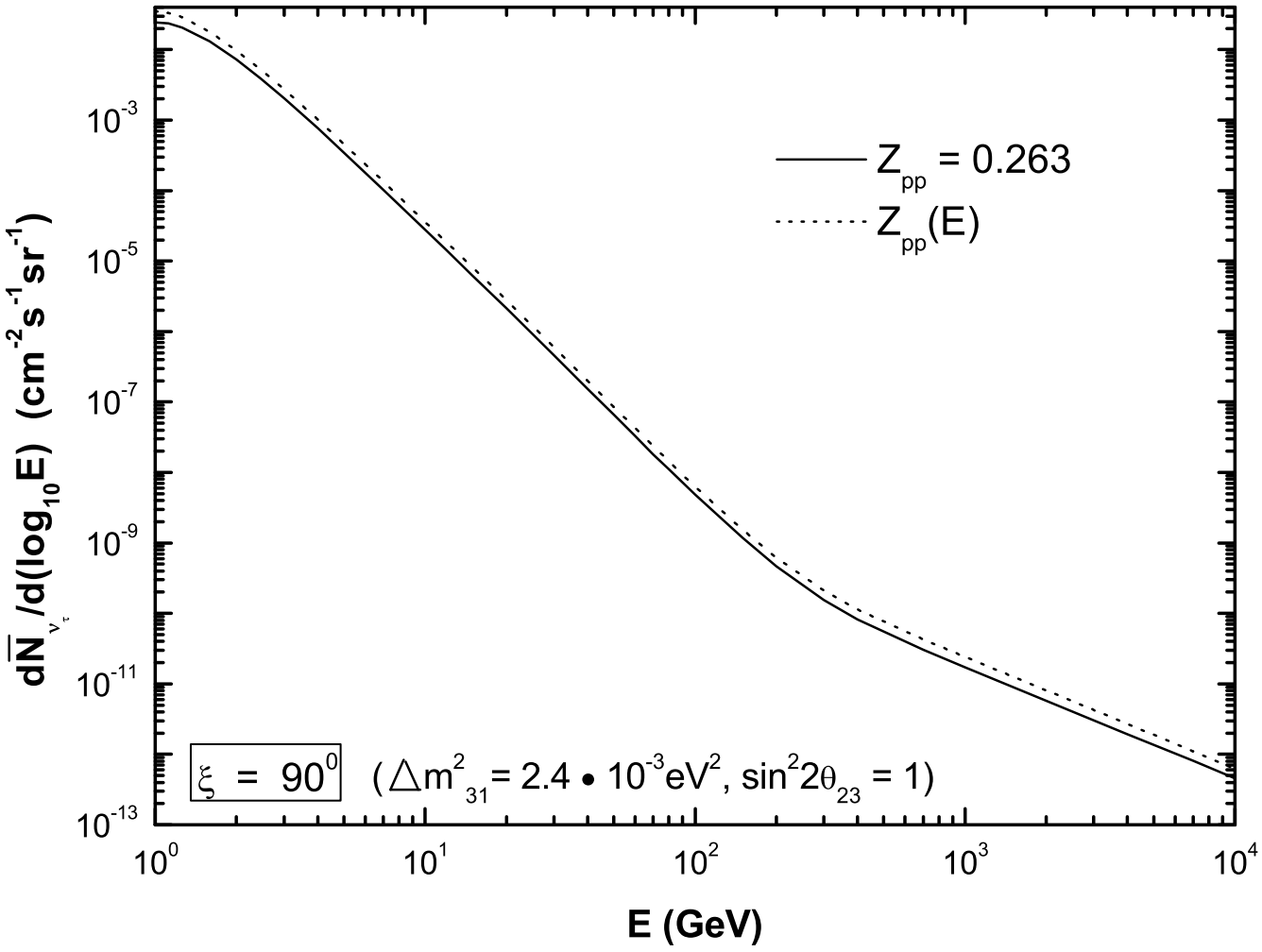

FIG. 9: The comparison of atmospheric ν_τ fluxes calculated from a constant Z_{pp} [12, 13] and an energy-dependent Z_{pp} [15] for $\xi = 90^\circ$.

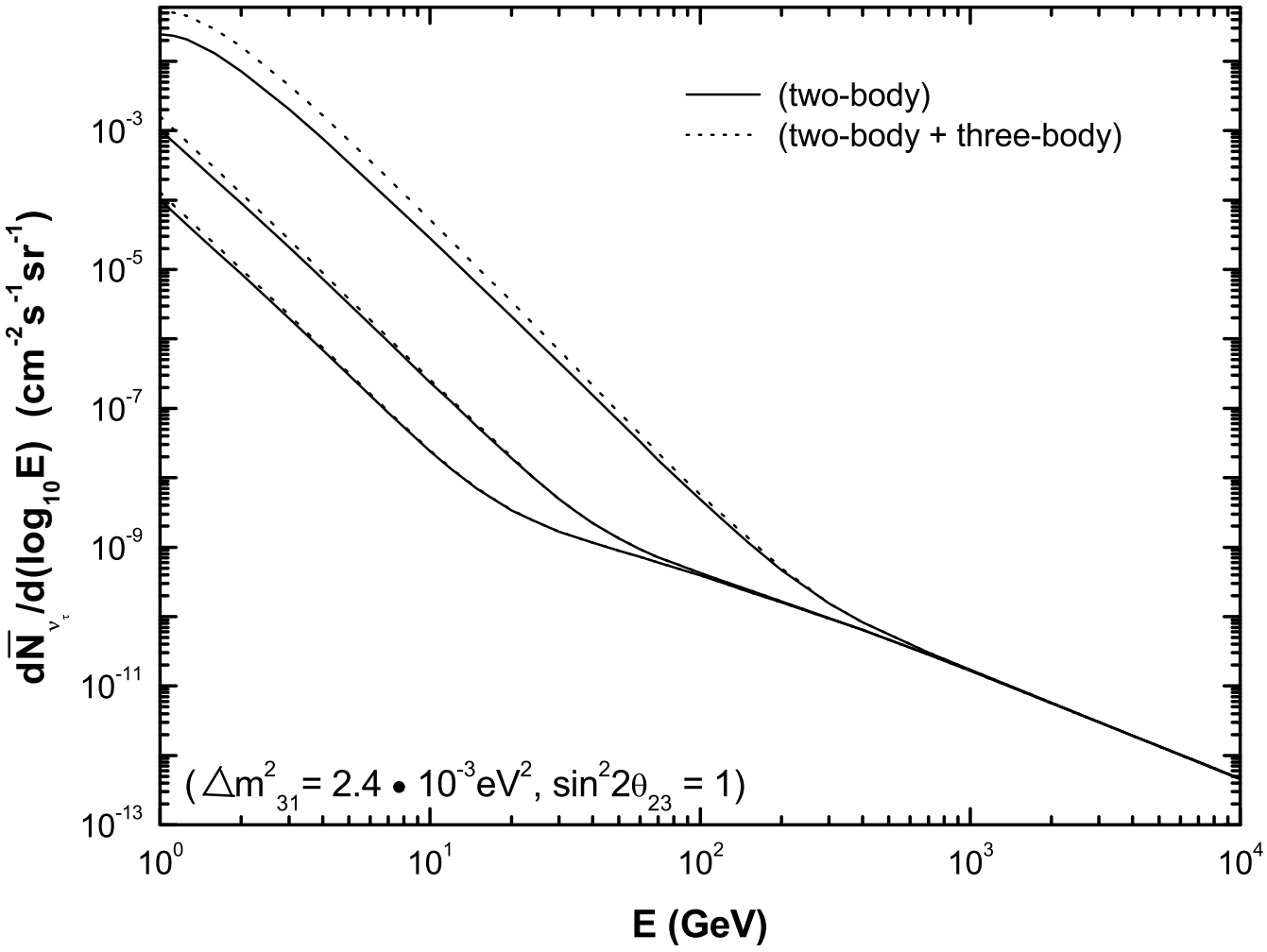

FIG. 10: The comparisons of atmospheric ν_τ fluxes resulting from the oscillations of ν_μ's generated by two-body and three-body decays with those resulting from the oscillations of ν_μ's generated only by two-body decays. The comparisons are made for three zenith angles, $\cos\xi = 0,\ 0.4$, and 1 (from top to bottom).

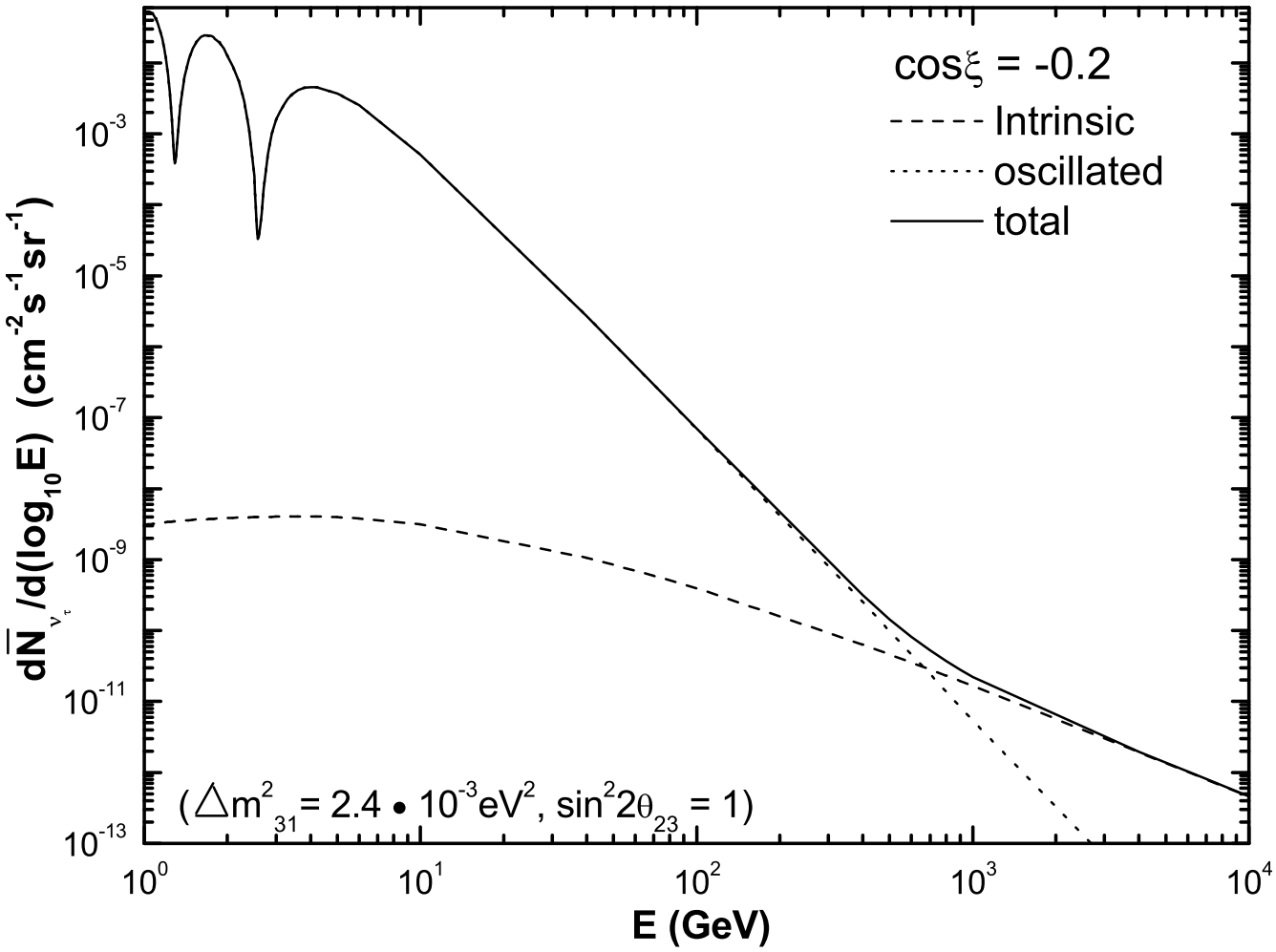

FIG. 11: The atmospheric ν_τ flux (solid line) as a sum of its oscillated (dotted line) and intrinsic (dashed line) components for $\cos\xi = -0.2$ with $\sin^2 2\theta_{23} = 1$, $\Delta m^2_{31} = 2.4 \cdot 10^{-3}$ eV^2, and $Z_{pp} = 0.263$.

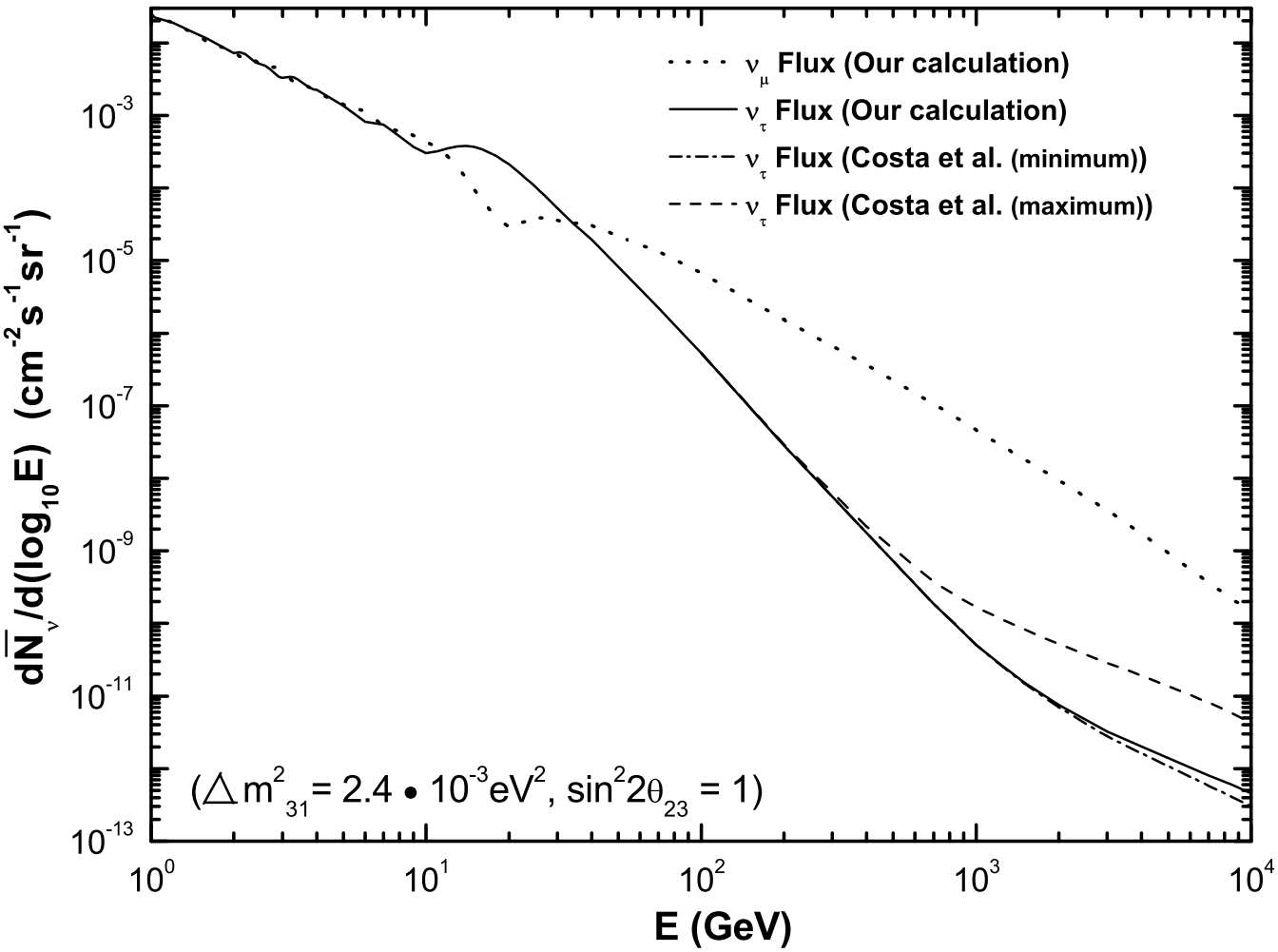

FIG. 12: The atmospheric ν_τ flux averaged for $-1 \leq \cos\xi \leq -0.4$. The uncertainty of this flux due to the uncertainty of intrinsic atmospheric ν_τ flux is shown. The corresponding ν_μ flux is also plotted, which is equal to the ν_τ flux for $1 \leq E/\mathrm{GeV} \leq 10$.

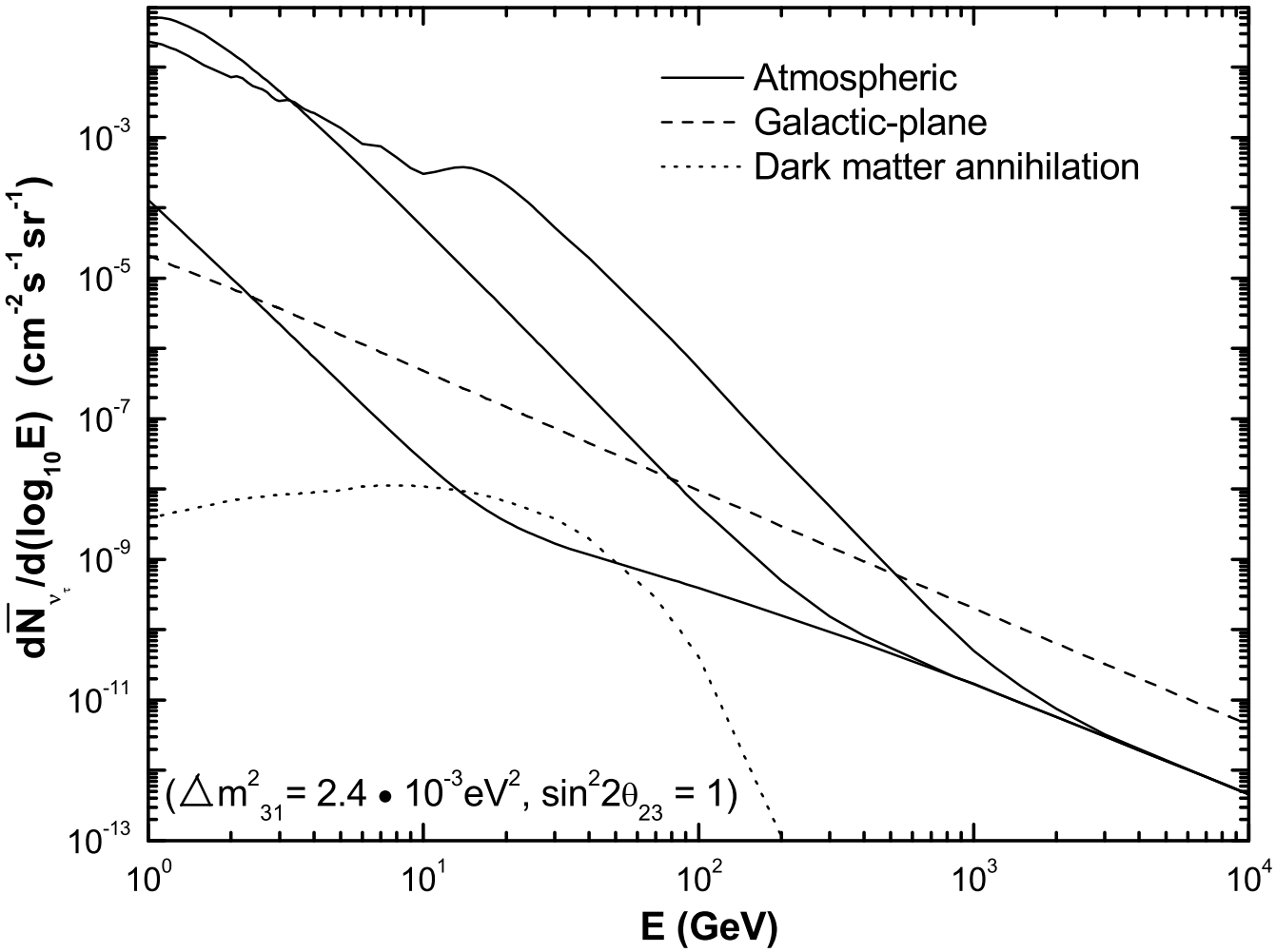

FIG. 13: The comparison of atmospheric ν_τ fluxes with the galactic-plane tau neutrino flux [10] and the tau neutrino flux due to the neutralino dark matter annihilations [32]. We have included downward ($\cos\xi = 1$), horizontal ($\cos\xi = 0$) and upward ($-1 \leq \cos\xi \leq -0.4$) atmospheric ν_τ fluxes for the comparison. At $E = 1$ GeV, the horizontal flux is the largest whereas the downward flux is the smallest.